Zeitschrift für Physikalische Chemie, **214**, 9, 1167−1186 (2000)

New Scheme for Measuring the Angular Momentum Spatial Anisotropy of Vibrationally Excited H_2 via the I $^1\Pi_g$ State

By Félix Fernández-Alonso, Brian D. Bean, James D. Ayers, Andrew E. Pomerantz and Richard N. Zare*

Department of Chemistry, Stanford University, Stanford, California 94305-5080, USA

Dedicated to Prof. Dr. Dr. h. c. mult. Jürgen Troe on the occasion of his 60th birthday

(Received April 20, 2000; accepted May 2, 2000)

H_2 Molecule / Vibrationally Excited / 2+1 REMPI / Rotational Anisotropy

We report the spectroscopic detection of vibrationally excited molecular hydrogen using 2+1 resonantly enhanced multiphoton ionization (REMPI) via the I $^1\Pi_g$ ($v' = 0$) − X $^1\Sigma_g^+$ ($v'' = 3$) band ca. 198 nm. Vibrationally excited H_2 was produced by passing room-temperature hydrogen over a hot ion gauge filament in a high-vacuum chamber. The internal energy distributions were characterized spectroscopically by use of the EF $^1\Sigma_g^+ - X\ ^1\Sigma_g^+$ 2+1 REMPI detection scheme. We have identified band origins for the S, Q, R, and P rotational branches of the I-X (0,3) band, as well as isolated lines corresponding to two-photon transitions into other nearby H_2 gerade states, including EF $^1\Sigma_g^+$ ($v' = 2, 3, 4$), GK $^1\Sigma_g^+$ ($v' = 1$), and J $^1\Delta_g$ ($v' = 0$). We propose the I-X transition as a suitable candidate for the determination of the rotational anisotropy of vibrationally excited ground-state H_2 molecules. We support this contention with a calculation of the line strength moments and sensitivities to the second- (quadrupolar) and fourth-rank (hexadecapolar) moments of the rotational angular momentum distributions, which is compared against the well-established Q-branch members of the EF $^1\Sigma_g^+ - X\ ^1\Sigma_g^+$ two-photon transition.

1. Introduction

The spectroscopic detection of ground-state hydrogen molecules is a difficult task. As a homonuclear diatomic molecule, the lack of a dipole moment does not permit the use of conventional infrared spectroscopy via electric-dipole-allowed transitions. Instead, it has been possible to use weak infrared

* Corresponding author. E-mail: zare@stanford.edu

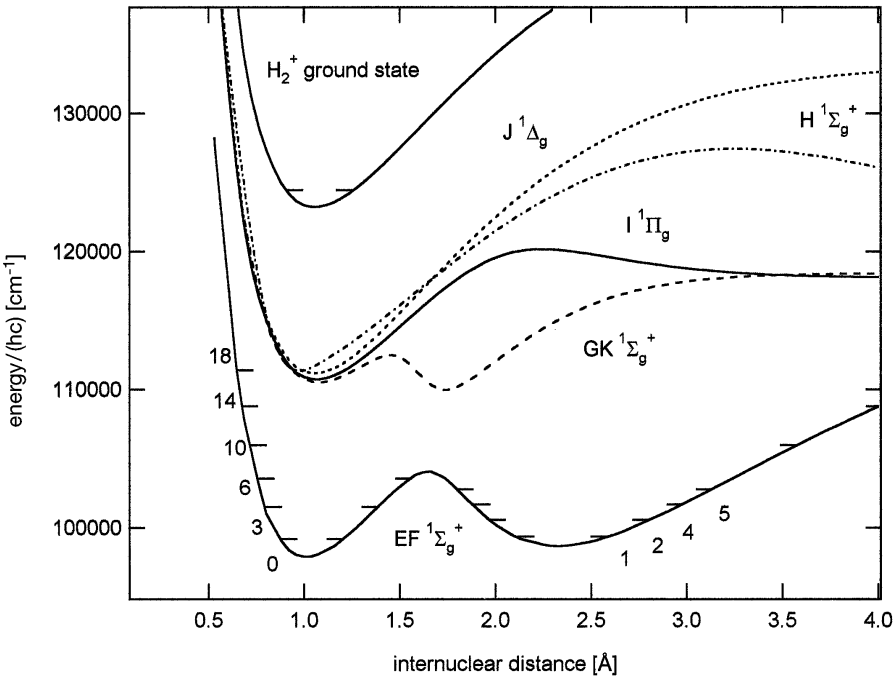

Fig. 1. Potential energy curves for several excited gerade electronic states of the H_2 molecule relevant to this work (taken from Wolniewicz and coworkers, see text for details). For reference, the position of the H_2^+ ion ground state has also been included.

quadrupole [1, 2] and Raman [3] transitions to perform the spectroscopic identification of the energy level structure of the ground electronic state of this molecule. The most favorable exception corresponds to the isotopomers HD, HT, and DT, with minute dipole moments ca. 10^{-4} Debye [4, 5].

The situation is marginally better for the case of electronic spectroscopy, because all excited-state transitions to bound electronic states lie in the vacuum ultraviolet (VUV). The recent availability of tunable VUV laser sources via nonlinear frequency mixing in rare gases [6] has fostered numerous studies of the excited states of hydrogen, particularly by the use of double-resonance VUV-VIS techniques [7−10].

A different approach for the detection of the hydrogen molecule involves the use of multiphoton spectroscopy using pulsed lasers and nonlinear frequency up-conversion. For the most typical case of two-photon spectroscopy, parity rules restrict its use to gerade excited states. Fig. 1 shows some of the gerade states relevant to this work and accessible via two-photon absorption around 170−250 nm. To date, only the intense, Q-branch members of the first four E-well vibrational bands of the EF $^1\Sigma_g^+ - X\ ^1\Sigma_g^+$

transition (cf. Fig. 1) have been fully characterized experimentally via 2+1 resonance enhanced multiphoton ionization (REMPI). These studies have allowed a quantitative determination of ground state rotational and vibrational distributions by Zare and coworkers [11−16]. The relative ease of implementation (i.e., only one laser is required) as well as the high sensitivity (ca. 10^{+5} molecules per cm^3 per quantum state [17, 18]) of this detection scheme makes it particularly attractive for applications involving low hydrogen molecule number densities. Such is the case for the study of the $H + H_2$ exchange reaction and its isotopic variants $D + H_2$ and $H + D_2$. Use of the aforementioned 2+1 REMPI scheme in our laboratory has permitted the determination of both quantum-state-specific integral [19−27] and differential cross section [28−31] in the past few years. Our most recent measurements of state-resolved differential cross sections for the $H + D_2 \rightarrow HD\ (v' = 3, J') + D$ reaction at 1.64 eV using the photoloc technique indicate a sensitivity under single-collision conditions to reactive scattering processes with cross sections as low as $10^{-3}-10^{-4}$ Å^2 [32].

The H_2 EF $^1\Sigma_g^+ - X\ ^1\Sigma_g^+$ Q branch, as well as those of N_2 a″ $^1\Sigma_g^+ - X\ ^1\Sigma_g^+$ [17, 33, 34] and CO B,C $^1\Sigma_g^+ - X\ ^1\Sigma_g^+$ [35], occupy a special place in the theory of two-photon line strengths for diatomic molecules. The magnetic-sublevel-averaged (M-averaged) line strengths for two-photon excitation with linearly polarized radiation contain both an isotropic (M-independent) and anisotropic (M-dependent) contribution [36−38]. Of these two terms, the isotropic one is generally much more intense resulting in a high detection sensitivity for this particular rotational branch. In marked contrast, its use to measure the spatial distribution of rotational angular momentum **J** is complicated by the implicit appearance of distinct virtual paths in the line strength expression and a general lack of sensitivity to the higher-order moments of the **J** distribution. Furthermore, a quantitative determination of the spatial distribution of angular momenta requires a careful measurement (or calculation) of radial dipole matrix elements, quantities that may prove quite elusive to pin down.

Until now, we have made extensive use of the Q-branch members of the EF $^1\Sigma_g^+ - X\ ^1\Sigma_g^+$ transition to measure the population (zeroth-order moment) of ground-state reaction products from the hydrogen-atom hydrogen-molecule bimolecular exchange reaction. For such a task, the EF $^1\Sigma_g^+ - X\ ^1\Sigma_g^+$ transition has proven superbly adequate. Nevertheless, it would be most desirable to have experimental access to higher-order moments of the **J** distribution. For example, a simultaneous measurement of the **J**-anisotropy and scattering-angle distributions of state-selected reaction products (the so-called **k**-**k**′-**J**′ triple vector correlation) will provide a most critical comparison between experiment and the most recent calculations [39] for this fundamental chemical reaction system. The field of stereodynamics has bloomed in the last few years and numerous examples exist for the measurement of the directional properties and attributes of photodissoci-

ation and reactive processes [40−43]. The hydrogen exchange reaction, however, still remains unexplored in this important aspect owing to the difficulty in carrying out these studies with presently available detection schemes.

On a more practical side, the appalling weakness of the O- and S-branch members of the EF $^1\Sigma_g^+ - X\ ^1\Sigma_g^+$ transition has prompted us to look for alternative 2+1 REMPI schemes via other nearby gerade excited states and with an inherently superior sensitivity to the higher-order moments of the **J** distribution. To fill the present lack of polarization-sensitive, two-photon transitions for the hydrogen molecule, we report the spectroscopic detection of vibrationally excited hydrogen molecules using 2+1 REMPI via the $I\ ^1\Pi_g$ ($v' = 0$) − $X\ ^1\Sigma_g^+$ ($v'' = 3$) band ca. 198 nm. We also compare this new detection scheme with the well-established Q-branch members of the EF $^1\Sigma_g^+ - X\ ^1\Sigma_g^+$ transition and show the suitability of the former for carrying out stereodynamical measurements in reactive scattering experiments.

2. Experimental

The experimental setup is the same as the one currently being used in our laboratory to measure quantum-state-resolved, center-of-mass differential cross sections for the $H + D_2 \rightarrow HD(v',J') + D$ exchange reaction using the photoloc technique. A detailed description of the experiment has already been given by Zare and coworkers [18, 29]. We limit ourselves to highlighting those elements relevant to the present study.

The experiments have been carried out in an ultrahigh vacuum (UHV) chamber. Typical base pressures are in the order of 8×10^{-8} torr and 4×10^{-8} torr in the ionization and detection regions respectively. The vacuum chamber houses a Wiley-McLaren time-of-flight spectrometer that enables ion mass separation prior to detection.

The ionization region is equipped with a nude ionization gauge (Granville Phillips 274-025) controlled by a Series 330 Ionization Gauge Controller (Granville Phillips). The emission current from the ionization gauge can be varied between 0.1 to 10 milliamperes. This nude ionization gauge is located approximately 23 cm away from the center of the ionization region and the chamber walls located immediately around it are water-cooled to maximize the production of vibrationally excited species.

High-purity hydrogen gas (Praxair 4.5 zero grade, 99.995% purity) is passed over the nude ion gauge filament at nominal ionization chamber pressures ranging between 5×10^{-5} and 1×10^{-4} torr. Pressures are kept constant within 2×10^{-6} torr by means of a dual-stage micrometer valve that allows for both coarse- and fine-flow adjustment. The mechanism for vibrational excitation of hydrogen is thought to proceed by molecular dissociation on the hot-filament surface followed by recombination, mostly on

the chamber walls [44−46]. We have used this source of vibrationally excited hydrogen molecules and isotopomers (HD and D_2) routinely in our reactive scattering experiments to locate the spectroscopic transitions of particular HD(v′,J′) quantum states [29].

The light source consists of a computer-controlled pulsed dye laser (Lambda Physik SCANMATE 2E) pumped by 115 mJ, 6 ns pulses of the second harmonic of an injection-seeded Nd:YAG laser (Spectra Physics GCR-4) running at 10 Hz. The nominal resolution of the laser, as determined by the grating, is 0.25 cm^{-1}. The doubling and mixing of the dye laser and/or the Nd:YAG fundamental frequencies is achieved in β-barium borate (BBO) and/or potassium diphosphate (KDP), type I crystals (Lambda Physik and INRAD), depending on the wavelength range we wish to cover. Typical output powers at the two-photon transition wavelengths ca. 195−200 nm were between 0.5−1.5 mJ/pulse. The laser beam was focused by a 600 mm fused-silica positive lens. Special care was exercised to operate with a well-defined beam polarization by use of a thin film polarizer (CVI Corporation) prior to focusing. Half- and quarter-wave plates (Optics for Research and CVI Corporation) located immediately after the polarizer and specifically designed to operate at these wavelengths were used to change the state of polarization of the beam. Wavelength scans were typically taken by integrating between 50 and 100 laser shots every 0.001 nm. An etalon (Larry Wolford Services, FSR = 1.0 cm^{-1}, finesse = 20, operating range 540−750 nm) was employed to check for laser scan nonlinearities in the recorded spectra. We determined that the maximum drift as the wavelength is scanned lies between 0.00050 and 0.00075 nm in the fundamental over the wavelength range of interest.

3. Results and discussion

3.1 Ion gauge characterization and experimental checks

As a first step in the search for new spectroscopic lines, we characterized the rotational distribution of H_2 ($v'' = 3$) via 2+1 REMPI through the EF $^1\Sigma_g^+$ ($v' = 0$) level. Zare and coworkers [14, 15] have investigated in detail this transition for the extraction of rotational populations. The major conclusion from their work was that the power-corrected line intensities should already mimic the rotational population because this particular branch possesses line strengths that depend very weakly on the initial rotational quantum number. Fig. 2a shows a raw spectrum of vibrationally "hot" H_2 ($v'' = 3$) produced by the hot filament at the maximum current setting. The line intensities show a characteristic alternation caused by the nuclear spin statistics of the H_2 molecule (a ratio of (I + 1)/I, with I = 1/2, favoring odd rotational levels). In Fig. 2b we display the relative rotational populations derived from the spectrum. The Boltzmann plot shown in Fig. 2c reveals a

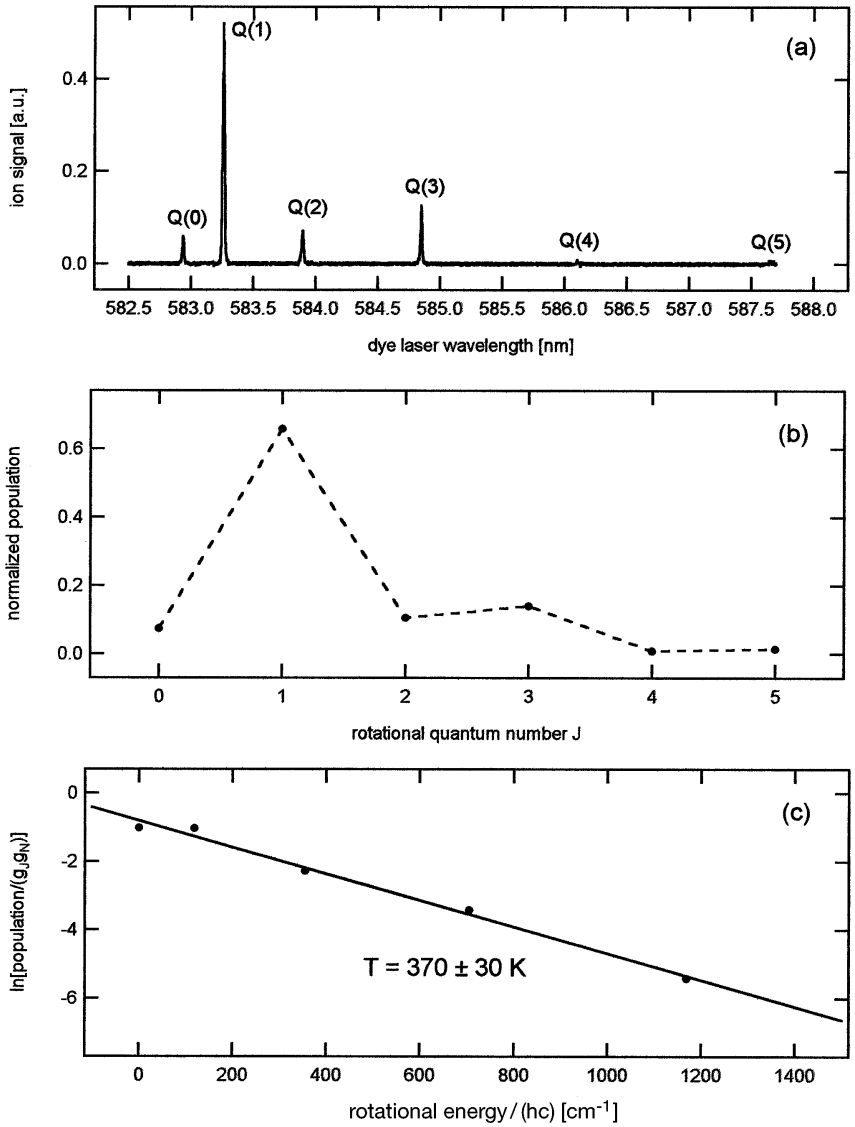

Fig. 2. (a) Ion-gauge H_2 2+1 REMPI spectrum via the Q-branch members of the EF $^1\Sigma_g^+ - X\ ^1\Sigma_g^+$ (0,3) band. (b) Relative rotational populations for ground state H_2 ($v'' = 3, J''$) derived from the spectrum shown in (a). (c) Boltzmann plot displaying a rotational temperature of 370±30 K.

rotational temperature close to room temperature. It is interesting to note the small degree of rotational excitation found from this source of internally excited hydrogen molecules. The rotational temperature observed for other

vibrational states and hydrogen molecule isotopomers is very similar to the one reported for H_2 ($v'' = 3$). This finding is in contrast with the amount of energy deposited in the vibrational degree of freedom. In the course of our investigations, we have observed up to H_2 ($v'' = 5$). Based on the signal levels detected for this high vibrational quantum number, we estimate that higher ones will still have a significant population. These relative rotational populations will be used later to extract line strength factors for newly identified spectral lines.

To verify the origin of the observed transitions, we have performed various experimental checks on the m/e = 2 ion signal. We deemed these additional checks necessary because H_2 spectra do not generally develop band heads and the precise determination of rotational progressions can become quite complicated. The most obvious and straightforward one is to scan over a given wavelength range with and without the hot ion gauge filament on. This check confirms the presence of spectroscopic features arising from hot bands of ground-state hydrogen molecules. Such a signal subtraction procedure is shown in Fig. 3a. In Fig. 3b we display the case of a coincidental spectral overlap between ion-gauge dependent ($v'' > 0$) and independent ($v'' = 0$) peaks. Subtraction of the two signals clearly shows a peak to the right of the ion-gauge-independent one arising from H_2 ($v'' > 0$). From our previous ion gauge rotational characterization studies we can be confident of the absence of high-rotation lines overlapping with the band origins of different vibrational progressions. This fact greatly simplifies the interpretation of the spectra.

As a final check on the identity of the observed lines we also performed polarization measurements. The simplest one, which compared signal intensities for excitation with linearly and circularly polarized light, is capable of differentiating between the Q-branch members of a $\Delta\Lambda = 0$ transition and all other possible transitions accessible via two-photon excitation. The intensity ratio for circular vs. linear polarization excitation for the Q branch of a $\Delta\Lambda = 0$ transition is given by:

$$\frac{I_{circ}}{I_{lin}} = \frac{3}{2}\left[\frac{A(J,\Lambda)}{A(J,\Lambda) + \dfrac{5\,\mu_i^2}{\mu_s^2}}\right] \tag{1}$$

where A(J) is a J- and Λ-dependent factor

$$A(J,\Lambda) = \frac{(J(J+1) - 3\,\Lambda^2)^2}{J(J+1)(2J-1)(2J+3)} \tag{2}$$

and μ_i^2/μ_s^2 is the ratio of the squares of two-photon transition dipoles [36]. For all the other branches of $\Delta\Lambda \neq 0$ transitions, circular polarization enhances the signal by a factor of 3/2, i.e., $\mu_i^2 = 0$ in Eq. (1). For example, the ratio μ_i^2/μ_s^2 approaches the value of ~25 for the EF $^1\Sigma_g^+ - X\ ^1\Sigma_g^+$ transition

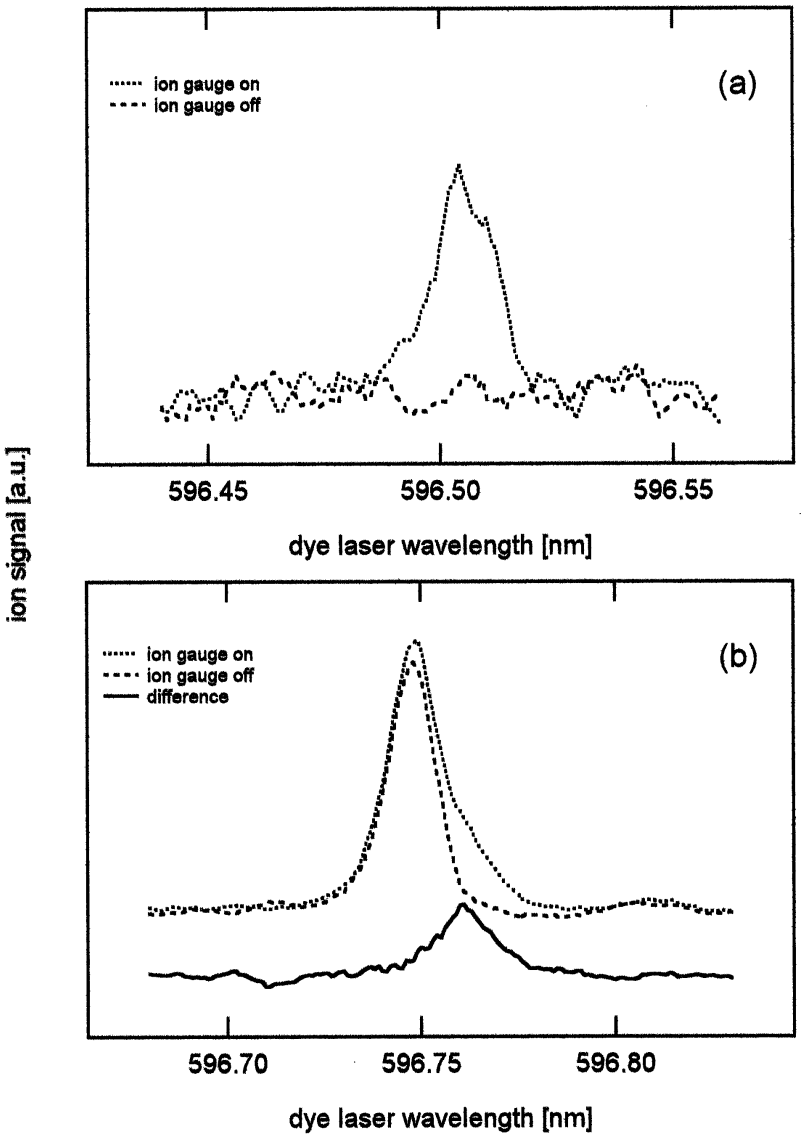

Fig. 3. (a) Illustration of an ion gauge "on-off" check employed to verify the origin of observed spectroscopic transitions. (b) Shows the case of a coincidental overlap (within our laser resolution) of an ion-gauge-dependent and independent peak. Subtraction of the two signals reveals the existence of a peak arising from vibrationally hot H_2 (solid line, vertically offset for clarity).

Table 1. H_2 molecule Franck-Condon factors for the electronic transitions relevant to this work.

Electronic transition	Prevalent character	Band (v′,v″)	Franck-Condon factor
EF $^1\Sigma_g^+ - X\ ^1\Sigma_g^+$	E (E0)	(0,0)	0.154
	E (E0)	(0,1)	0.355
	E (E0)	(0,2)	0.324
	E (E0)	(0,3)	0.142
	E (E0)	(0,4)	0.035
	F(F0)	(1,0)	1.37e-7
	F (F1)	(2,0)	8.28e-7
	E (E1)	(3.0)	0.189
	F (F2)	(4,0)	0.001
	F (F3)	(5,0)	0.001
	E (E2)	(6,0)	0.123
	E (E2)	(6,0)	0.123
I $^1\Pi_g - X\ ^1\Sigma_g^+$	I	(0,0)	0.071
	I	(0,1)	0.238
	I	(0,2)	0.325
	I	(0,3)	0.233
GK $^1\Sigma_g^+ - X\ ^1\Sigma_g^+$	K (K0)	(0,3)	0.009
	G (G0)	(1,3)	0.239
J $^1\Delta_g - X\ ^1\Sigma_g^+$	J	(0,3)	0.219

[18] and similar ratios are expected for other $^1\Sigma_g^+ - ^1\Sigma_g^+$ transitions in the H_2 molecule. Consequently, the intensity ratio shown in Eq. (1) will depart from the more usual value of 3/2. In our case, spectroscopic lines showing an intensity ratio of circular to linear polarization of 3/2 will arise from either $\Sigma-\Pi$ (I state) or $\Sigma-\Delta$ (J state) transitions, whereas those with a ratio smaller than 3/2 will be from $\Sigma-\Sigma$ transitions (EF, GK, H states). Furthermore, we found that for those lines not having a polarization ratio approaching 3/2, linear polarization was more effective than circular. This finding implies $\mu_i^2/\mu_s^2 \gg 1$ and $I_{circ}/I_{lin} \ll 1$, in agreement with what is expected for a typical $\Sigma-\Sigma$ transition. This polarization check has been used to confirm and/or further corroborate the spectroscopic assignments based on line positions presented in the next section.

3.2 Spectroscopic assignments

To gain insight into the possible transitions from ground-state $H_2(v'')$ levels that may fall into our two-photon frequency range (99 500 − 101 000 cm^{-1}), we have computed Franck-Condon (FC) factors (see Table 1) for several spectroscopic bands involving the EF $^1\Sigma_g^+$, I $^1\Pi_g$, GK $^1\Sigma_g^+$, and J $^1\Delta_g$ states.

We note that our assignment of vibrational quantum numbers for the double-well states EF $^1\Sigma_g^+$ and GK $^1\Sigma_g^+$ does not follow previous naming conventions that assumed vibrational progressions for each potential energy well [47, 48]. We have chosen to assign vibrational quantum numbers based on the number of nodes in the vibrational wavefunction following the convention of Huo and Jaffe [49]. The vibrational quantum numbers for the EF $^1\Sigma_g^+$ state are displayed in Fig. 1 and show an alternation of vibrational quantum numbers between the E and F wells. For reference purposes we have included in Table 1 a column indicating the prevalent character of a given vibrational level (which potential energy well holds the largest wavefunction amplitude) as well as the alternative vibrational quantum label often found in the literature, i.e., E0, E1, F1, etc. The potential energy curves employed for this calculation, which have been plotted in Fig. 1, have been obtained from the extensive theoretical *ab initio* calculations of Wolniewicz and coworkers on the H_2 molecule [50−55]. The H_2^+ ion ground-state potential energy curve was taken from the work of Bates *et al.* [56]. The rotationless ($J = 0$) radial Schrödinger equation was integrated using the Numerov algorithm [57] to solve for the eigenenergies and eigenfunctions. For the double-well states, we followed the eigenvalue search procedure extensively discussed by Wolniewicz [58] and by Johnson [59].

Huo *et al.* [15] have shown that it is not generally valid to rely on FC factors when considering two-photon excitation. At the same time, however, it was found that the FC factors for the EF $^1\Sigma_g^+$ ($v' = 0$) − X $^1\Sigma_g^+$ (v'') transition are quite similar to the computed *ab initio* values. We, therefore, took the FCs as qualitative guides in the determination of the most important vibronic bands contributing to our spectrum. The FC factors shown in Table 1 are quite favorable for transitions ending in vibrational states of the ground state greater than zero and follow a similar trend to those of the EF $^1\Sigma_g^+$ ($v' = 0$) − X $^1\Sigma_g^+$ (v'') bands. For example, the FC factor for the I $^1\Pi_g$− X $^1\Sigma_g^+$(0,3) band is 3.3 times larger than that for the (0,0) band. For the double-well states, excitation to the outer wells is very weak even for the GK $^1\Sigma_g^+$ ($v' = 0$), centered at an internuclear distance approximately halfway between the E and F wells of the EF $^1\Sigma_g^+$ state (see Fig. 1). Our biggest unknown is the electronic transition dipole moments, quantities that require a full *ab initio* calculation. These quantities have only been calculated by Huo *et al.* [15] for the EF $^1\Sigma_g^+$−X $^1\Sigma_g^+$ two-photon transition. At present we have no means of calculating or estimating these values. It is hoped that this work will encourage others to calculate the two-photon transition strengths connecting the ground state to these higher-lying gerade states.

Absolute frequency calibration was performed by using the term energies and transition energies for the EF $^1\Sigma_g^+$ ($v' = 3$) (E1) reported by Eyler *et al.* [60]. The accuracy of Eyler's values is 0.01 cm^{-1}, sufficient given our experimental resolution. Our scanning step and excitation bandwidth in the VUV are 0.17 cm^{-1} and 1.4−1.5 cm^{-1} respectively, the latter one as in-

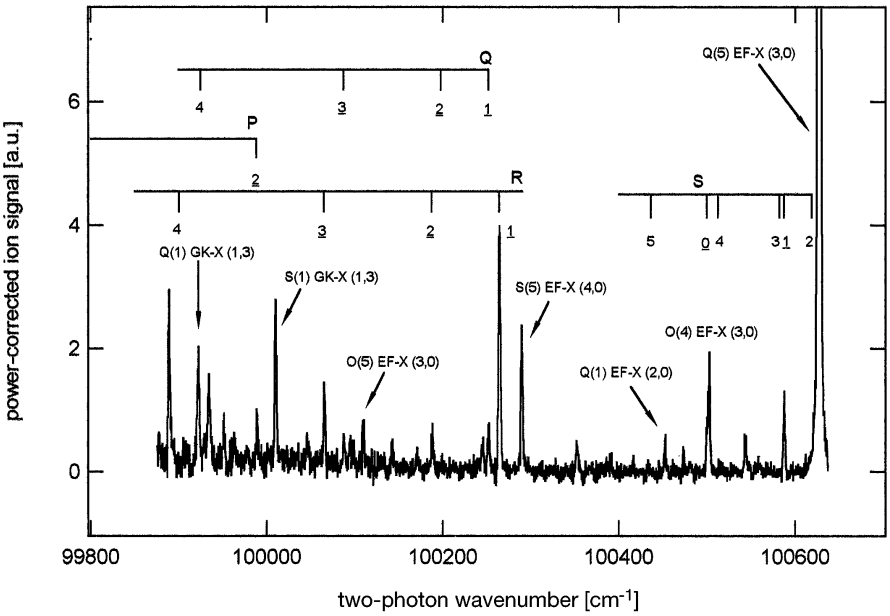

Fig. 4. Power-corrected 2+1 REMPI spectrum vs. total transition energy (two-photon frequency) and spectroscopic assignments. The P, Q, R, and S branches shown correspond to the I $^1\Pi_g - X\ ^1\Sigma_g^+$ (0,3) band. Rotational lines from these branches and detected in this study are underlined. Other isolated lines and their corresponding spectroscopic assignments are also shown.

ferred from the peak widths. Taking into account the frequency jitter in our laser (see experimental section), we estimate a measurement accuracy of the H_2 line centers of $0.3-0.4\ cm^{-1}$ at the two-photon energies. Furthermore, the presence of three EF $^1\Sigma_g^+$ ($v' = 3$) − X $^1\Sigma_g^+$ ($v' = 0$) lines in our spectrum (see Fig. 4) permits a further check of the wavelength scan linearity in addition to the use of the etalon (see experimental section). The experimental (ion gauge on-off, polarization ratios) checks described in section III 3.1 were used to verify the identity of each of the assignments reported. Ground-state energies for H_2 were taken from Schwartz and Le Roy [61]. For the ground-state energy levels used throughout our work, these values are within $0.1\ cm^{-1}$ to those previously reported by Dabrowski [62] and by Herzberg and Howe [63]. All three sets of ground-state energies give the same results within our frequency resolution.

A power-corrected 2+1 REMPI spectrum vs. absolute two-photon frequency is shown in Fig. 4, which gives the positions of the P-, Q-, R-, and S-branch members of the H_2 I $^1\Pi_g$ ($v' = 0$) − X $^1\Sigma_g^+$ ($v'' = 3$) band. Two-photon excitation causes O, P, Q, R, and S rotational branches to appear in

Table 2. Transition energies/(hc) and assignments for observed $H_2I\ ^1\Pi_g - X\ ^1\Sigma_g^+$ (0,3) 2+1 REMPI rotational lines.

Observed (cm^{-1})	Jungen *et al.*[1] (cm^{-1})	$\Delta_{Jungen\text{-}observed}$ (cm^{-1})	Assignment
100500.32	100499.95	−0.37	S(0)*
100587.85	100587.62	−0.23	S(1)
100264.11	100264.20	0.09	R(1)
100187.77	100187.47	−0.30	R(2)
100065.46	100065.09	−0.37	R(3)
100252.38	100251.82	−0.56	Q(1)
100197.96	100197.68	−0.29	Q(2)
100087.16	100087.03	−0.13	Q(3)
99988.42	99988.25	−0.17	P(2)

* Blended with EF-X (3,0) O(4). See Fig. 3a and Table 3.

[1] Ch. Jungen, I. Dabrowski, G. Herzberg and M. Vervloet, J. Chem. Phys. **93** (1990) 2289.

the spectrum. Moreover, parity rules for the two-photon step dictate that O, Q, and S branches can only connect the ground-state $^1\Sigma_g^+$ with $^1\Pi_g^+$ whereas P and R branches connect to $^1\Pi_g^-$ [1, 36, 37]. Of these two possible upper electronic states, the minus Λ-doublet is expected to show the least amount of perturbation from nearby electronic states according to the well-known selection rules $\Delta J = 0$, $\Delta S = 0$, $\Delta J = 0 \pm 1$, and $+ \leftrightarrow + / - \leftrightarrow -$ [64]. We expect that P and R branches will have both line positions and intensities more in agreement with *ab initio* calculation and the theory of two-photon line strengths.

Table 2 shows the observed transition frequencies for the $I\ ^1\Pi_g$ ($v' = 0$) − $X\ ^1\Sigma_g^+$ ($v'' = 3$) band and their comparison with the values derived from the term energies of Jungen *et al.* [65]. The differences between Jungen's and our values all lie within our experimental resolution with the probable exception of the Q(1) line ($-0.56\ cm^{-1}$). This discrepancy may be caused by our inability to determine the peak position with higher precision, especially if there is a coincidental overlap with another spectral line at this frequency. If this is the case, the overlapping line is also arising from vibrationally excited H_2, which was confirmed by an on-off ion gauge check. Furthermore, it does not arise from a Q branch of a $\Sigma - \Sigma$ transition because the circular-to-linear polarization ratio is the expected value of 3/2.

We list in Table 3 the assignment for additional line positions. Those corresponding to the EF $^1\Sigma_g^+$ ($v' = 3$) − $X\ ^1\Sigma_g^+$ ($v'' = 0$) transition are the ones that have been used as frequency markers, especially the most intense one corresponding to Q(5). The assignments corresponding to the GK $^1\Sigma_g^+$, and $J\ ^1\Delta_g$ states remain tentative because we have not observed other branch

Table 3. Additional transition energies/(hc) and assignments for observed H_2 2+1 REMPI rotational lines.

Observed (cm^{-1})	Other work[1, 2] (cm^{-1})	$\Delta_{other-observed}$ (cm^{-1})	Assignment
100626.91	100626.91	(frequency marker)	EF-X(3,0) Q(5)
100502.93	100502.82	−0.11	EF-X(3.0) O(4)
100289.42	100289.40	−0.02	EF-X(4,0) S(5)
100009.75	100009.67	−0.08	GK-X(1,3) S(1)*
100109.20	100109.14	−0.06	EF-X(3,0) O(5)
100452.45	100452.32	−0.13	EF-X(2,0) Q(1)**
100452.45	100452.14	−0.32	J-X(0,3) Q(2)**
99922.14	99921.69	−0.45	GK-X(1,3) Q(1)*

* Tentative assignment.

** Signal has both gauge-dependent and gauge-independent contributions (blended line).

[1] EF state term energies from E. E. Eyler, J. Gilligan, E. McCormack, A. Nussenzweig and E. Pollack, Phys. Rev. A **36** (1987) 3486, and P. Senn, P. Quadrelli, K. Dressler and G. Herzberg, J. Chem. Phys. **83** (1985) 962.

[2] GK and J state term energies from Ch. Jungen, I. Dabrowski, G. Herzberg and M. Vervloet, J. Chem. Phys. **93** (1990) 2289.

members and some of them suffer from coincidental overlaps with ion-gauge-independent lines.

3.3 Sensitivity to rotational polarization

To determine whether the I $^1\Pi_g - X\ ^1\Sigma_g^+$ transition can be used to perform polarization measurements, it is necessary to obtain more quantitative information about the observed line strengths and to compare these to the ones expected from the theory of two-photon transitions. The rotational populations have been obtained from the ion-gauge characterization studies presented in section III3.1. Once we take these populations into account, we find that the observed line strengths for different rotational branches do not follow the expected ratios. More specifically, the P and R on the one hand and the Q and S branches on the other agree with each other but the Q-P, S-P etc. do not. This finding immediately suggests that the line strengths independently follow the theoretical line strength positions for each Λ doublet. The Q and S branches corresponding to the Π^+ doublet are weaker by about a factor of ten than the P and R branches corresponding to the Π^- doublet. This intensity discrepancy might be caused by differences in the intermediate state character or in the efficiency of the ionization step. A knowledge of the wave function character of the energy levels of this parity doublet as well as an explicit calculation of two-photon line strengths will help elucidate whether it is possible to use the usual two-photon line

strength factors for the Q and S branches. If this is the case, then it may still be possible to use these branches to measure the rotational polarization. As a simple experimental check, a given polarization parameter for the same ground-state J level could be measured in two different branches (i.e., R/P and Q/S).

So far we have paid little attention to the role of the ionization step. In our case, the nature of the 2+1 REMPI process generally ensures the saturation of this step because relatively high laser fluences are required to drive the resonant two-photon step. This situation is typically the case for the EF $^1\Sigma_g^+ - X\ ^1\Sigma_g^+$ transition. Nevertheless, such a saturation condition should be experimentally checked (i.e., the measured ion signal is quadratic in laser power) because it is highly dependent on experimental factors such as beam spatial and temporal profiles, focusing condition, etc. Moreover, the fact that only one photon effects the ionization of the molecule makes this particular REMPI scheme more suitable and possibly more sensitive than other well-studied $\Sigma - \Pi$ transitions such as, for example, 2+2 REMPI of N_2 via the a $^1\Pi_g$ state [66−71].

We would like to provide a comparison of the expected sensitivities to the angular momentum spatial anisotropy for the observed I $^1\Pi_g - X\ ^1\Sigma_g^+$ 2+1 REMPI scheme. For such a purpose we use the formalism developed by Kummel, Sitz and Zare [38, 72] using spherical tensor moments [73] and the Hertel-Stoll convention [74]. In the case of a a two-photon resonant transition using linearly polarized light it is possible to write the observed intensity I as

$$I = C_{\text{det}} \sum_{k,q} P_q^k (J_i, \Lambda_i, J_f, \Lambda_f, \Omega)\, A_q^k(J_i) \tag{3}$$

where the P_q^k coefficients are the moments of the line strength, the A_q^k values are the spherical moments of the ground state distribution, and C_{det} is a detector sensitivity constant. The A_q^k values characterize the spatial distribution of angular momenta $\mathbf{J_i}$ with, for example, A_0^0, A_0^1, A_0^2, and A_0^4 being the monopolar (population), dipolar, quadrupolar, and hexadecapolar moments. The moments of the line strength P_q^k are coefficients dependent on the initial rotational quantum number and the type of transition, as well as on the excitation-detection geometry that we denote by the collective index Ω. The range of index k in Eq. (3) depends on the number and state of polarization of the photons involved in the resonant step. For a two-photon (n = 2) transition using idential photons (i.e., same laser) we are only sensitive to the even k moments up to the k = 2n = 4. These moments of the line strength P_q^k can be regarded as geometry-dependent sensitivities to a particular spherical tensor component A_q^k.

Kummel, Sitz and Zare [38, 72] have tabulated the complete expressions to calculate the moments of the line strength for any type of two-photon transition characterized by initial quantum numbers J_i and Λ_i. In general, calculation of these factors does not involve more than extensive angular

momentum algebra with the exception of the Q branch of a $\Delta\Lambda = 0$ transition. For our particular case of the EF $^1\Sigma_g^+ - X\ ^1\Sigma_g^+$ transition, we do also need to know the relative contributions of the $\Sigma-\Sigma-\Sigma$ ($\Delta\Lambda = 0$ followed by $\Delta\Lambda = 0$) and $\Sigma-\Pi-\Sigma$ ($\Delta\Lambda = +1$ followed by $\Delta\Lambda = -1$ or *vice versa*) virtual paths when evaluating the sum over intermediate levels. This quantity can be inferred from a comparison of O-/S- vs. Q-branch intensities in a H_2 spectrum of known rotational population, i.e., room-temperature sample, or by comparing the circular-to-linear-polarization intensity ratio of a Q-branch line. Such a measurement permits a determination of μ_i^2/μ_s^2, which in our case is $\sim$25 (see section III3.1). The relationship between μ_i^2/μ_s^2 and the ratio of radial dipole matrix elements ϱ for the two distinct virtual paths is given by

$$\varrho = \frac{R_{ei}^o R_{fe}^o}{R_{ei}^{\pm 1} R_{fe}^{\mp 1}} = \frac{1 + \dfrac{\mu_i}{\mu_s}}{\dfrac{1}{2} - \dfrac{\mu_i}{\mu_s}} \tag{4}$$

where $R_{xy}^{\Delta\Lambda}$ is a radial dipole moment integral for a single-photon transition between electronic states x and y, and characterized by a change in the projection of the electronic angular momentum $\Delta\Lambda = 0, \pm 1$. The subscripts i, e, and f denote the initial, intermediate, and final electronic states respectively. On the left-hand side of Eq. (4) the numerator corresponds to the $\Sigma-\Sigma-\Sigma$ and the denominator to the $\Sigma-\Pi-\Sigma$ paths. The fraction μ_i/μ_s can be either positive or negative because we have only measured the ratio of their squares, i.e., we have not measured the relative phases between the two transition amplitudes. This leads to two possible ratios of radial terms of -1.33 and -0.73. These ratios have been explicitly included in the calculation of the moments of the line strength P_q^k.

In Fig. 5 we show the behavior of the normalized P_0^2 and P_0^4 moments of the line strength for $J_i = 3$ as a function of the angle between the polarization of the laser and the detection axis for the case of an orthogonal excitation-detection geometry (the one typically employed in our reactive scattering experiments). Fig. 5a corresponds to the EF $^1\Sigma_g^+ - X\ ^1\Sigma_g^+$ and Fig. 5b to the $I\ ^1\Pi_g - X\ ^1\Sigma_g^+$ transition. For the case of the EF $^1\Sigma_g^+ - X\ ^1\Sigma_g^+$ Q branch, the experimental sensitivity (intensity variation with polarization angle) to the second and fourth-order moments is very small. Also note the opposite sign but very similar magnitude for the two virtual path ratios used for the EF $^1\Sigma_g^+ - X\ ^1\Sigma_g^+$ Q branch. Furthermore, the $\Pi-\Sigma$ sensitivities are considerably larger than those computed for the $\Sigma-\Sigma$ Q branch, for the second and even more so for the fourth moments of the line strength.

In these calculations, we have not included the effects of hyperfine (nuclear spin) depolarization (HFD) and, therefore, they should be regarded as

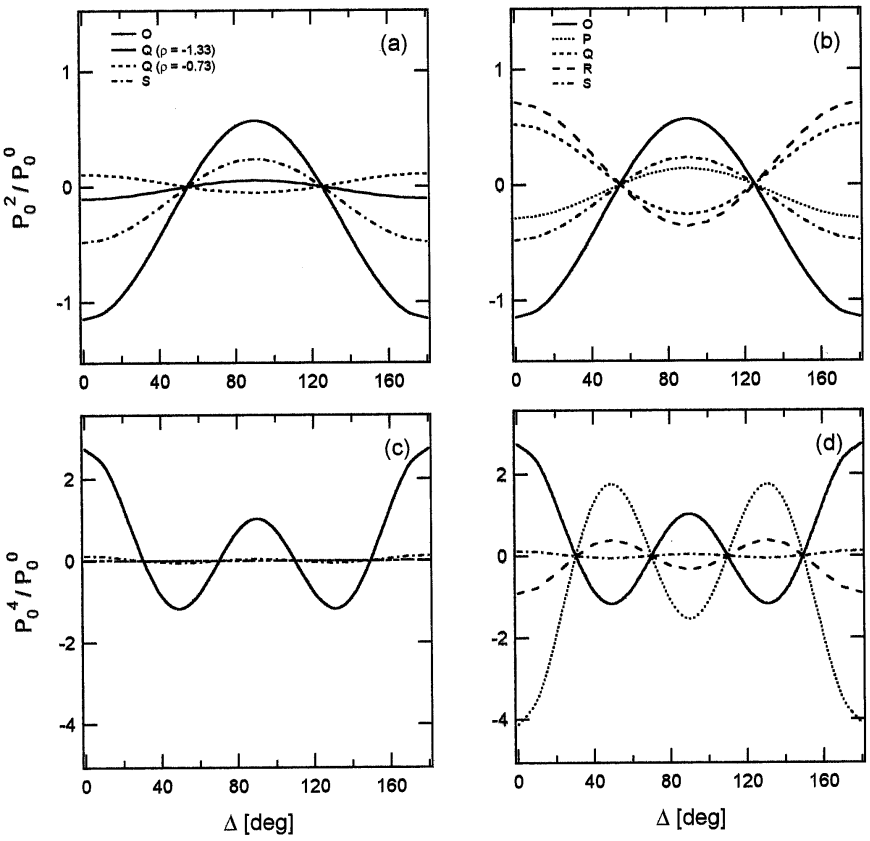

Fig. 5. Normalized quadrupolar (P_0^2) and hexadecapolar (P_0^4) moments of the line strength vs. polarization angle Δ for H_2 ($J'' = 3$). (a), (c) correspond to EF $^1\Sigma_g^+ - X\ ^1\Sigma_g^+$ (left) and (b), (d) to I $^1\Pi_g - X\ ^1\Sigma_g^+$ (right). The Q-branch EF $^1\Sigma_g^+ - X\ ^1\Sigma_g^+$ moments of the linestrength have been computed for the two virtual path ratios consistent with our measurements (see text for details).

strict upper estimates of the sensitivity to the rotational anisotropy. We, however, expect HFD to be minor because the nuclear spin-rotation interaction in H_2 is -133.9 ± 0.01 KHz [75]. The precise value of the HFD factor for a given J depends on the rank k of the angular distribution moment as well as on the temporal delay between formation and detection (i.e., photolysis-probe delay in our experiments) [76−78]. If we ascribe a characteristic timescale τ ($\tau^{-1} \sim$ hyperfine coupling constant) to HFD, we immediately see that the associated timescales are in the order of 7−8 μs whereas typical photolysis-probe delays in photoinitiated reactive scattering experiments are 10−50 ns.

Table 4. Sensitivities s^k (k = 2, 4) for EF $^1\Sigma_g - X\ ^1\Sigma_g^+$ and I $^1\Pi_g - X\ ^1\Sigma_g^+$ rotational branches.

	EF $^1\Sigma_g - X\ ^1\Sigma_g^+$	I $^1\Pi_g - X\ ^1\Sigma_g^+$				
J	Q	O	P	Q	R	S
1*	−0.072/0.069**	0	0	−0.447	0.447	−0.125
	0/0	0	0	0	0	0
3	−0.047/0.047	−0.511	−0.127	0.234	0.319	−0.213
	0.002/0.002	0.914	1.371	0.914	−0.305	0.042
6	−0.044/0.045	−0.406	0.029	0.296	0.255	−0.255
	0.002/0.002	0.339	−0.873	0.872	−0.400	0.071
12	−0.044/0.045	−0.361	0.097	0.313	0.219	−0.284
	0.002/0.002	0.218	−0.707	0.861	−0.472	0.097
24	−0.043/0.045	−0.340	0.129	0.318	0.188	−0.301
	0.002/0.002	0.176	−0.634	0.858	−0.517	0.117

* For each J, first and second rows correspond to sensitivity to second- and fourth-rank polarization moments.

** First and second entries correspond to virtual state path ratios of −1.33 and −0.73 (see text for details).

To complete our comparison of the EF $^1\Sigma_g^+ - X\ ^1\Sigma_g^+$ Q branch and I $^1\Pi_g - X\ ^1\Sigma_g^+$ transitions we have included in Table 4 the normalized sensitivities to the second and fourth order moments of the **J** distribution. The sensitivities s^k can be obtained from the expression for the moments of the line strength P_q^k following Zare and coworkers [38, 72]

$$P_q^k = s^k(J_i, \Lambda_i, J_f, \Lambda_f)\ Y_q^k(\Delta, 0) \tag{5}$$

where $Y_q^k(\Delta,0)$ is a spherical harmonic of rank k and component q. Note that the angular dependence shown by Eq. (5) is clearly fulfilled by the normalized moments of the line strength shown in Fig. 5. In analogy with our previous discussion for the P_q^k's, the values given in Table 4 have been normalized by the zeroth-order value so as to provide an indication of the relative contribution of each term to the overall intensity. Comparison between both electronic transitions show an increase by at least a factor of five and as high as an order of magnitude for the sensitivity to the second and fourth-order moments of the **J** distribution in favor of the I $^1\Pi_g - X\ ^1\Sigma_g^+$ transition. Such a trend holds up to the classical, high-J limit.

In typical measurements of reactive product polarization, the measured laboratory-frame anisotropy is the result of an implicit averaging over all possible scattering frames contributing to the measured reaction signal. This averaging results in a reduction of the observed anisotropy in comparison to the one associated with the physically relevant scattering frame [79]. Consequently, the use of a sensitive and versatile spectroscopic transition to perform this type of measurements becomes an almost-mandatory pre-

requisite to progress beyond the current state of the art for the fundamental $H + H_2$ exchange reaction. We believe the $I\ ^1\Pi_g - X\ ^1\Sigma_g^+\ 2+1$ REMPI detection scheme we have reported may become such a tool.

Acknowledgments

We thank Larry Wolford for loaning to us the visible etalon used in the examination of the laser wavelength scan reproducibility. Elf-Atochem (Brian D. Bean), the Hertz Foundation and Stanford University (James D. Ayers), and the National Science Foundation (Andrew E. Pomerantz) are gratefully acknowledged for support in the form of Graduate Fellowships. This work was supported by the U.S. National Science Foundation under Grant Number CHE-99-00305.

References

1. G. Herzberg, *Molecular Spectra and Molecular Structure*, Krieger Publishing Co., Malabar, reprinted in (1989).
2. S. L. Bragg, J. W. Brault and W. H. Smith, Astrophys. J. **263** (1982) 999.
3. D. K. Veirs and G. M. Rosenblatt, J. Mol. Spec. **121** (1987) 401.
4. P. Essenwanger and H. P. Gush, Can. J. Phys. **62** (1984) 1680.
5. M.-C. Chuang and R. N. Zare, J. Mol. Spec. **121** (1987) 380.
6. C. R. Vidal, in *Tunable Lasers*, Vol. 59, Springer-Verlag Topics in Applied Physics (1987) pp. 57−113.
7. E. Reinhold, W. Hogervorst, W. Ubachs and L. Wolniewicz, Phys. Rev. A **60** (1999) 1258.
8. H. Suzuki, M. Nakata, Y. Ogi and K. Tsukiyama, J. Mol. Spec. **191** (1998) 142.
9. E. Reinhold, A. de Lange, W. Hogervorst and W. Ubachs, J. Chem. Phys. **109** (1998) 9772.
10. K. Tsukiyama, J. Ishii and T. Kasuya, J. Chem. Phys. **97** (1992) 875.
11. E. E. Marinero, C. T. Rettner and R. N. Zare, Phys. Rev. Lett. **48** (1982) 1323.
12. E. E. Marinero, R. Vasudev and R. N. Zare, J. Chem. Phys. **78** (1983) 692.
13. K.-D. Rinnen, D. A. V. Kliner, R. N. Zare and W. M. Huo, Isr. J. Chem. **29** (1989) 369.
14. K.-D. Rinnen, M. A. Buntine, D. A. V. Kliner and R. N. Zare, J. Chem. Phys. **95** (1991) 214.
15. W. M. Huo, K.-D. Rinnen and R. N. Zare, J. Chem. Phys. **95** (1991) 205.
16. A. J. R. Heck, W. M. Huo, R. N. Zare and D. W. Chandler, J. Mol. Spec. **173** (1995) 452.
17. K. R. Lykke and B. D. Kay, J. Chem. Phys. **95** (1991) 2252.
18. F. Fernández-Alonso, Ph.D. Thesis, Stanford (1999).
19. E. E. Marinero, C. T. Rettner and R. N. Zare, J. Chem. Phys. **80** (1984) 4142.
20. R. S. Blake, K.-D. Rinnen, D. A. V. Kliner and R. N. Zare, Chem. Phys. Lett. **153** (1988) 365.
21. K.-D. Rinnen, D. A. V. Kliner, R. S. Blake and R. N. Zare, Chem. Phys. Lett. **153** (1988) 371.
22. D. A. V. Kliner, K.-D. Rinnen and R. N. Zare, Chem. Phys. Lett. **166** (1990) 107.
23. D. A. V. Kliner and R. N. Zare, J. Chem. Phys. **92** (1990) 2107.
24. D. A. V. Kliner, D. E. Adelman and R. N. Zare, J. Chem. Phys. **94** (1991) 1069.
25. D. E. Adelman, N. E. Shafer, D. A. V. Kliner and R. N. Zare, J. Chem. Phys. **97** (1992) 7323.

26. D. Neuhauser, R. S. Judson, D. J. Kouri, D. E. Adelman, N. E. Shafer, D. A. V. Kliner and R. N. Zare, Science **257** (1992) 519.
27. D. E. Adelman, H. Xu and R. N. Zare, Chem. Phys. Lett. **203** (1993) 573.
28. H. Xu, N. E. Shafer-Ray, F. Merkt, D. J. Hughes, M. Springer, R. P. Tuckett and R. N. Zare, J. Chem. Phys. **103** (1995) 5157.
29. F. Fernández-Alonso, B. D. Bean and R. N. Zare, J. Chem. Phys. **111** (1999) 1022.
30. F. Fernández-Alonso, B. D. Bean and R. N. Zare, J. Chem. Phys. **111** (1999) 1035.
31. F. Fernández-Alonso, B. D. Bean and R. N. Zare, J. Chem. Phys. **111** (1999) 2490.
32. F. Fernández-Alonso, B. D. Bean, J. D. Ayers, D. E. Pomerantz, R. N. Zare, L. Bañares and F. J. Aoiz, Angewandte Chemie International Edition **30** (2000) 2748.
33. T. F. Hanisco and A. C. Kummel, J. Phys. Chem. **95** (1991) 8565.
34. T. F. Hanisco, C. Yan and A. C. Kummel, J. Phys. Chem. **96** (1992) 2982.
35. P. J. H. Tjossem and K. C. Smyth, J. Chem. Phys. **91** (1989) 2041.
36. R. G. Bray and R. M. Hochstrasser, Mol. Phys. **31** (1976) 1199.
37. K.-m. Chen and E. S. Yeung, J. Chem. Phys. **69** (1978) 43.
38. A. C. Kummel, G. O. Sitz and R. N. Zare, J. Chem. Phys. **85** (1986) 6974.
39. M. P. de Miranda, F. J. Aoiz, L. Bañares and V. S. Rábanos, J. Chem. Phys. **111** (1999) 5368.
40. *Issue on the Sterodynamics of Chemical Reactions*, J. Phys. Chem. A **101** (1997) 7461.
41. A. J. Orr-Ewing and R. N. Zare, Annu. Rev. Phys. Chem. **45** (1994) 315.
42. *Richard B. Bernstein Memorial Issue on Molecular Dynamics*, J. Phys. Chem. A **95** (1991) 7961.
43. G. E. Hall and P. L. Houston, Annu. Rev. Phys. Chem. **40** (1989) 375.
44. R. I. Hall, I. Cadez, M. Landau, F. Pichou and C. Schermann, Phys. Rev. Lett. **60** (1988) 337.
45. P. J. Eenshuistra, J. H. M. Bonnie, J. Los and H. J. Hopman, Phys. Rev. Lett. **60** (1988) 341.
46. D. C. Robie, L. E. Jusinski and W. K. Bischel, Appl. Phys. Lett. **56** (1990) 722.
47. T. E. Sharp, Atomic Data **2** (1971) 119.
48. D. J. Kliger and C. K. Rhodes, Phys. Rev. Lett. **40** (1978) 309.
49. W. M. Huo and R. L. Jaffe, Chem. Phys. Lett. **101** (1983) 463.
50. W. Kolos and L. Wolniewicz, J. Chem. Phys. **43** (1965) 2429.
51. W. Kolos and L. Wolniewicz, J. Chem. Phys. **50** (1969) 3228.
52. L. Wolniewicz and K. Dressler, J. Mol. Spec. **67** (1977) 416.
53. K. Dressler and L. Wolniewicz, Can. J. Phys. **62** (1984) 1706.
54. W. Kolos and J. Rychlewski, J. Mol. Spec. **91** (1982) 128.
55. L. Wolniewicz and K. Dressler, J. Chem. Phys. **100** (1994) 444.
56. D. R. Bates and R. H. G. Reid, Adv. At. Mol. Phys. **4** (1968) 13.
57. T. Pang, *Introduction to Computational Physics*, Cambridge University Press, Cambridge (1997).
58. L. Wolniewicz, J. Chem. Phys. **51** (1969) 5002.
59. B. R. Johnson, J. Chem. Phys. **67** (1977) 4086.
60. E. E. Eyler, J. Gilligan, E. McCormack, A. Nussenweig and E. Pollack, Phys. Rev. A **36** (1987) 3486.
61. C. Schwartz and R. J. Le Roy, J. Mol. Spec. **121** (1987) 420.
62. I. Dabrowski, Can. J. Phs. **62** (1984) 1639.
63. G. Herzberg and L. L. Howe, Can. J. Phys. **37** (1959) 636.
64. H. Lefevre-Brion and R. W. Field, *Perturbations in the Spectra of Diatomic Molecules*, Academic Press, Orlando (1986).
65. Ch. Jungen, I. Dabrowski, G. Herzberg and M. Vervloet, J. Chem. Phys. **93** (1990) 2289.
66. G. O. Sitz, A. C. Kummel and R. N. Zare, J. Vac. Sci. Technol. A **5** (1987) 513.
67. G. O. Sitz, A. C. Kummel and R. N. Zare, J. Chem. Phys. **89** (1988) 2558.

68. G. O. Sitz, A. C. Kummel, R. N. Zare and J. C. Tully, J. Chem. Phys. **89** (1988) 2572.
69. A. C. Kummel, G. O. Sitz, R. N. Zare and J. C. Tully, J. Chem. Phys. **89** (1988) 6947.
70. A. C. Kummel, G. O. Sitz, R. N. Zare and J. C. Tully, J. Chem. Phys. **91** (1989) 5793.
71. B. Girard, G. O. Sitz, R. N. Zare, N. Billy and J. Vigué, J. Chem. Phys. **97** (1992) 26.
72. A. C. Kummel, G. O. Sitz and R. N. Zare, J. Chem. Phys. **88** (1988) 6707.
73. U. Fano and J. H. Macek, Rev. Mod. Phys. **45** (1973) 553.
74. V. Hertell and W. Stoll, Adv. At. Mol. Phys. **13** (1978) 113.
75. C. H. Townes and A. L. Schawlow, *Microwave Spectroscopy*, Dover Publications, Inc., New York (1975).
76. R. Altkorn, Ph.D. Thesis, Stanford (1984).
77. R. Altkorn, R. N. Zare and C. H. Greene, Mol. Phys. **55** (1985) 1.
78. A. J. Orr-Ewing, W. R. Simpson, T. P. Rakitzis and R. N. Zare, Isr. J. Chem. **34** (1994) 95.
79. N. E. Shafer-Ray, A. J. Orr-Ewing and R. N. Zare, J. Phys. Chem. **99** (1995) 7591.